Exploration of a simple, low cost, micro gas turbine recuperator solution for a domestic combined heat and power unit

A Clay, G.D. Tansley

Accepted Manuscript

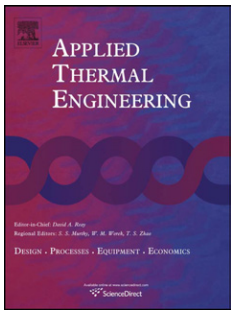

Title: Exploration of a simple, low cost, micro gas turbine recuperator solution for a domestic combined heat and power unit

Authors: A Clay, G.D. Tansley

PII: S1359-4311(11)00238-9

DOI: 10.1016/j.applthermaleng.2011.04.037

Reference: ATE 3533

To appear in: *Applied Thermal Engineering*

Received Date: 25 September 2010

Revised Date: 13 April 2011

Accepted Date: 22 April 2011

Please cite this article as: A Clay, G.D. Tansley. Exploration of a simple, low cost, micro gas turbine recuperator solution for a domestic combined heat and power unit, Applied Thermal Engineering (2011), doi: 10.1016/j.applthermaleng.2011.04.037

Exploration of a simple, low cost, micro gas turbine recuperator solution for a domestic combined heat and power unit

A Clay[*], and **GD Tansley**
School of Engineering and Applied Science, Aston University, Birmingham, United Kingdom

Abstract:

For Micro Gas Turbines (MGT) of around 1 kW or less, a commercially suitable recuperator must be used to produce a thermal efficiency suitable for use in UK Domestic Combined Heat and Power (DCHP).

This paper uses Computational Fluid Dynamics (CFD) to investigate a recuperator design based on a helically coiled pipe-in-pipe heat exchanger which utilises industry standard stock materials and manufacturing techniques. A suitable mesh strategy was established by geometrically modelling separate boundary layer volumes to satisfy y^+ near wall conditions. A higher mesh density was then used to resolve the core flow.

A coiled pipe-in-pipe recuperator solution for a 1 kW MGT DCHP unit was established within the volume envelope suitable for a domestic wall-hung boiler. Using a low MGT pressure ratio (necessitated by using a turbocharger oil cooled journal bearing platform) meant unit size was larger than anticipated. Raising MGT pressure ratio from 2.15 to 2.5 could significantly reduce recuperator volume.

Dimensional reasoning confirmed the existence of optimum pipe diameter combinations for minimum pressure drop. Maximum heat exchanger effectiveness was achieved using an optimum or minimum pressure drop pipe combination with large pipe length as opposed to a large pressure drop pipe combination with shorter pipe length.

Keywords:

micro gas turbine, domestic combined heat and power, micro combined heat and power, pipe in pipe, heat exchanger, micro recuperator, coiled, helically, CFD, DCHP, MGT

[*] Corresponding author: Mechanical Engineering and Design, School of Engineering and Applied Science, Aston University, Aston Triangle, Birmingham, B4 7ET, UK. email: claya@aston.ac.uk

1. Introduction

Suitable prime movers for DCHP must be cheap, reliable and operate with a high thermal efficiency [1]. When possible, they should also run continuously to promote electricity generation for export to maximise end user financial income. Internal combustion engines require linear to rotary power transfer and so cannot run continuously without regular maintenance. Stirling engines are simple but sealing, external combustion heat addition and balancing result in an expensive, heavy and complex unit. Fuel cells produce the highest thermal efficiencies but installation and maintenance costs remain too high for reasonable payback periods. Gas turbines favour continuous running to avoid temperature gradients and have fewer components resulting in a smaller, lighter, cheaper and more compact unit. Whilst other MGT investigations have advanced technological development [2] [3], attention towards reducing unit cost has yet to be addressed.

Following a review of prior recuperator art; Micro channel [4] [5], Stamp and folded [6], Offset-strip-fin [7], Corrugated plate fin – RSAB recuperator [8] [9], Annular – Capstone [10], Swiss roll [11] [12], Rolls-Royce spiral recuperator [13] [14], ACTE spiral recuperator [15] [14] and speculative investigation into alternative recuperator proposals [16] a coiled pipe-in-pipe recuperator was selected for further investigation.

The heat exchange boundary between two fluid streams is easily realised with a simple counter-flow pipe-in-pipe arrangement. However, in most applications the required pipe length to provide adequate heat exchange effectiveness is unpractical; this is especially so for DHCP applications. Typically, for a simple cycle gas turbine, the components: bearing unit, compressor, turbine and generator are aligned on a single shaft along the axial direction. For a compact solution, the obvious way to arrange the recuperator is annually, surrounding the components, which also provides a safety zone in case of blade-off failure. Geometrically, a coiled pipe-in-pipe heat exchanger best lends itself to a MGT recuperator application as components can be positioned within the central void, see Figure 1, whilst commercially the use of stock materials and established manufacturing processes is clearly beneficial to minimise costs.

2. Concept

2.1 Theory

Bending two pipes of different diameter on the same pitch and Neutral Axis Bend Diameter (NABD), would allow the small pipe to be positioned or screwed inside the large pipe, to form the separate fluid zones, see Figure 2. Welding end pieces will force the pipes to sit concentrically after being stiffened from coiling. With very little welding and material manipulation, it is envisaged that the unit cost of this solution will come close to the target 1.5 × material cost target for commercialisation [6].

To assess recuperator suitability, target hydraulic and thermal performance requirements (pressure drop and heat exchanger effectiveness) were established using the fundamental recuperated gas turbine equations;

$$\eta_s = \frac{\eta_b |W_{net}|}{\Delta H_{53} \times f} \quad \textbf{(1)}$$

$$|W_{net}| = |W_{out}| - |W_{in}| \quad \textbf{(2)}$$

$$|W_{out}| = C_{pg}(T_{03} - T_{04}) \quad \textbf{(3)}$$

$$|W_{in}| = \left(\frac{1}{\eta_m}\right) C_{pa}(T_{02} - T_{01}) \quad \textbf{(4)}$$

$$f = \frac{\left(C_{pa}(T_{03} - T_{05})\right)}{\left(\eta_b \Delta H_{53} - C_{pg} T_{03}\right)} \quad \textbf{(5)}$$

$$\eta_{HEX} = \frac{(T_{05} - T_{02})}{(T_{04} - T_{02})} \quad \textbf{(6)}$$

$\Delta H_{53} = 43{,}100$ [kJ/kg] [17]

Putting equations 2, 3, 4, 5, and 6 into 1 we arrive at equation 7.

$$\eta_s = \frac{\eta_b \left(C_{pg}(T_{03} - T_{04}) - \frac{C_{pa}}{\eta_m}(T_{02} - T_{01}) \right) \left(\eta_b \Delta H_{53} - C_{pg} T_{03}\right)}{\Delta H_{53} C_{pa} \left(T_{03} - T_{02}(1 - \eta_{HEX}) + T_{04} \eta_{HEX}\right)} \quad \textbf{(7)}$$

$$T_{02} - T_{01} = \frac{T_{01}}{\eta_c}\left(\left(\frac{P_{02}}{P_{01}}\right)^{\left(\frac{\gamma_a - 1}{\gamma_a}\right)} - 1\right) \quad \textbf{(8)}$$

$$T_{03} - T_{04} = T_{03}\eta_t\left(1 - \left(\frac{P_{03}}{P_{04}}\right)^{\left(\frac{1-\gamma_g}{\gamma_g}\right)}\right) \quad \textbf{(9)}$$

$$\left(\frac{P_{03}}{P_{04}}\right)^{\left(\frac{1-\gamma_g}{\gamma_g}\right)} = \left(\frac{P_{02}\left(1 - \frac{\Delta P_{ha}}{P_{02}} - \frac{\Delta P_b}{P_{02}}\right)}{P_{01}\left(1 + \frac{\Delta P_{hg}}{P_{01}}\right)}\right)^{\left(\frac{1-\gamma_g}{\gamma_g}\right)} \quad \textbf{(10)}$$

$$\frac{P_{02}}{P_{01}} = r_c \quad \textbf{(11)}$$

$$P = \frac{\left(1 - \frac{\Delta P_{ha}}{P_{02}} - \frac{\Delta P_b}{P_{02}}\right)}{\left(1 + \frac{\Delta P_{hg}}{P_{01}}\right)} \quad \textbf{(12)}$$

Putting equations 11 into 8 and 10, 11, 12 into 9, then 8 and 9 into 7 we arrive at equation 13

$$\eta_s = \frac{\eta_b\left(C_{pg}T_{03}\eta_t\left(1 - \left(r_c P\right)^{\left(\frac{1-\gamma_g}{\gamma_g}\right)}\right) - \frac{C_{pa}}{\eta_m}\frac{T_{01}}{\eta_c}\left(r_c^{\left(\frac{\gamma_a - 1}{\gamma_a}\right)} - 1\right)\right)\left(\eta_b \Delta H_{53} - C_{pg}T_{03}\right)}{\Delta H_{53}C_{pa}\left(T_{03} - T_{01}\left(\frac{1}{\eta_c}\left(r_c^{\left(\frac{\gamma_a - 1}{\gamma_a}\right)} - 1\right) + 1\right)\left(1 - \eta_{HEX}\right) + T_{03}\eta_{HEX}\left(1 - \eta_t\left(1 - \left(r_c P\right)^{\left(\frac{1-\gamma_g}{\gamma_g}\right)}\right)\right)\right)} \quad \textbf{(13)}$$

Where, heat exchanger effectiveness, η_{HEX}, is given by equation 6 and pressure drop ratio, P, by equation 12. The pressure drop ratio, P, is a dimensionless parameter used to assess the pressure drop within the hot and cold streams or inner pipe and annulus collectively. A similar approach to Equation 13 has been demonstrated in [4] [18] where attention is given to optimizing hot and cold side pressure drops.

Equation 13 describes recuperated gas turbine performance by the hydraulic and thermal performance or pressure drop ratio, P, and heat exchanger effectiveness,

η_{HEX} , of the recuperator. Using a defined set of MGT parameters [19]: η_s =15%, r_c =2.15, η_c =73%, η_t =75%, η_m =90%, η_b =98%, T_{01} =288 K, T_{03} =1200 K, C_{pa} =1005 kJ/kg-K, C_{pg} =1148 kJ/kg-K, γ_a =1.40, γ_g =1.33, target recuperator hydraulic/thermal performance requirements can be established for a particular MGT system as illustrated in Figure 3.

Figure 3 shows a less demanding recuperator performance can provide the same system efficiency with a higher pressure ratio, r_c. A similar conclusion was made in [20] which, along with the importance of a high pressure ratio, highlighted the need for a larger pressure drop to be located on the cold side combined with a larger hydraulic diameter on the hot side where the atmospheric pressure differential was smallest.

At work outputs of 1 kW or less, pressure ratios greater than 2.15 requires shaft speeds up to 500,000 rev/min [3] that must be accommodated for by air bearing technology, which at these scales has yet to be proven commercially. A pressure ratio, r_c, of 2.15 at, η_c =75%, was theoretically demonstrated using lower shaft speeds (170,000 – 200,000 rev/min) within the realms of oil cooled journal bearings found on turbochargers [21]. This produced a system efficiency, η_s, of 15%, using a heat exchanger effectiveness, η_{HEX}, of 75% which from Figure 3 is shown to require a pressure drop ratio, P, of 90% or more. Other test based theoretical predictions of similar sized/duty MGT suggest system efficiencies between 16%-20% [22] and 6%-13.5% [23] are possible.

2.2 Practical Considerations

For this study it was assumed that all pipe diameters could be coiled on a minimum radius of 1.5 × pipe diameter. Although 90° fitting s at this bend radius exist, coiling on this radius would be pushing current technological limits. All material was modelled as stainless steel heat exchanger tube Standard Wire Gauge (SWG) 22 (0.711 mm thick) or 18 (1.218 mm thick) where appropriate. Table 1 shows the tube combinations investigated.

3. Coiled Pipe Heat Transfer State-Of-The-Art

A broad literature review of heat transfer in curved pipes can be found in [24] additional work which has directly influenced this study is briefly reviewed here. Due

to the development of complex secondary toroidal flow patterns, coiled pipe-in-pipe heat exchangers are used in applications where additional heat transfer is required for a pressure drop penalty. The coil bend radius governs the magnitude of centrifugal force imposed on the moving fluid, while the coil pitch influences torsion [25]. Increased torsion promotes turbulent flow [26] which is advantages in heat transfer. Compared to a straight pipe, critical Reynolds or Dean number (coiled pipe equivalent) decreased to between 500 and 600 when the dimensionless torsion value, β_0, was increased up to an optimum of 1.3, after which critical Dean number began to rise again [26] [27]. Flow observations have shown increased torsion to diminish the anticlockwise vortex and strengthen the clockwise vortex which, following the right hand rule, is in the same direction as the applied torsion. The twin toroidal distortion from continually increased torsion eventually leads to cross section velocity flow profiles similar to a straight pipe [27].

Experimental work of coiled pipe flow was conducted in the 70's and 80's but visual confirmation of the twin vortex toroidal flow structure was first demonstrated in [28]. Results of CFD simulations with varied flow rates and pipe diameters were presented in [29] supported by experimental data from literature. The modelling technique in the present study, outlined in section 4, is similar to the test validated technique described in [30] with the refinements discussed later in [31] and the adoption of coupled heat transfer wall boundaries rather than constant wall heat flux to more accurately reflect heat transfer between the different fluids [32]. Improvements with regard to more accurate mesh control are described and demonstrated in Section 4.3.

4. CFD methodology

4.1 Geometry definition

For the pipe geometry, an algorithm was written in Matlab[1] which produced .txt and .jou files for export into Gambit[2] (CFD geometry modelling software). The .txt file contained global coordinate vertex points, whilst the .jou contained instructions to construct geometry, apply mesh and assign boundary/fluid zones. The code was fully

[1] The Mathworks, Inc., 3 Apple Hill Drive, Natick, MA 01760-2098, USA. Version 7.6.0 (R2008a).

[2] ANSYS, Inc., Southpointe, 275 Technology Drive, Canonsburg, PA 15317, USA. Gambit version 2.4.6.

automated based on the following input parameters; coil pitch, coil diameter, number of turns, pipe diameters, pipe thickness, pipe cross section element density and pipe length element number.

Each annulus section was divided into 3 equal cross sectional volumes, whilst the inner pipe remained as a single volume. This provided the most stable geometry both during construction and meshing. Tetrahedral elements were used for the inner pipe cross section and quadrilateral for all annulus cross sections. The following mesh strategy was used to ensure negative volumes were not created: each pipe cross section face at one end and the walls of the inner pipe were meshed before the faces were stitched to create the volumes. Once stitched, the inner pipe fluid volume was meshed followed by each surrounding annulus volume which allowed mesh transfer to each new pipe wall.

4.2 CFD Boundary Conditions

Fluent[3] was used to computationally model momentum and heat transfer in the coiled pipe geometries. Both the pipe and annulus were modelled with mass flow inlets and pressure outlets. Input, output and target values for mass flow, temperature and pressure were established from MGT system calculations, see Table 2. Each heat transfer surface was modelled as separate wall boundaries to enable thermal coupling between the separated heat transfer medians instead of a constant heat flux condition which was found to be inaccurate [25].

Each fluid was modelled as air as the exact combustion products of the exhaust gas were not known. Density was calculated by ideal gas law, specific heat was calculated by a piecewise polynomial function using 8 coefficients for each of the ranges between 100 K to 1000 K and 1001 K to 3000 K from [33]. Thermal conductivity and viscosity were both modelled as piecewise linear functions.

A double precision, pressure based solver was used. The RNG k-ε viscous model with Differential Viscosity Model, Viscous Heating and Full Buoyancy Effects were invoked. A near wall treatment method was deemed suitable for the flow behaviour encountered here, provided the y^+ wall boundary criteria was met. To more accurately predict heat transfer by accounting for pressure gradients from complex flows that may involve separation, the 2 layer Non-Equilibrium Wall Functions model was used over the Standard Wall Functions model. With relatively little skewness,

[3] ANSYS, Inc., Southpointe, 275 Technology Drive, Canonsburg, PA 15317, USA. Fluent version 6.3

SIMPLE Pressure-Velocity Coupling was chosen over PISO. With elements aligned to the direction of flow and a structured grid over a long duct of constant diameter, numerical diffusion would be relatively small [34]. As such, First Order Upwind discretization would probably have provided fast and stable solutions with good convergence. However, to maintain consistency with other literature Second Order Upwind discretization was used for each equation. Under-relaxation factors for each equation were set to 0.6 except pressure which was set at 0.3.

4.3 Grid sensitivity

Grid sensitivity with respect to boundary layer and heat transfer is associated with the pipe cross sectional area element number, whilst sensitivity with respect to development length is associated with the pipe length element number. For this study, grid sensitivity is based on pipe cross section as achieving the correct mesh density to satisfy near wall treatment criteria is essential for accurate results. To establish gird sensitivity, temperature and pressure change between inlet and outlet were recorded for a single turn with increasing grid densities.

A grid density of 31.7 elements/cm^3 was validated against experimental heat transfer data to within 2% error [30] using the modelling strategy previously described. When wall treatment methods are used, y^+ values should be around 30 or in the range $30<y^+<300$ but always >11.2 to avoid viscosity calculations in the laminar sub layer where the semi-empirical wall treatment functions are instead used under the k-ε viscosity model.

The definition of empirical wall treatments means y^+ values are influenced both by the cross sectional near-wall grid density and the Reynolds number or flow speed with faster media more able to facilitate finer near wall girds. Whilst a sufficient grid density is required to resolve the core flow, excessive grid densities with small y^+ values will not accommodate the 2 layer empirical relationships used for turbulence modelling and should be avoided.

To ensure the wall y^+ criteria would be met, whilst retaining a sufficient mesh density to resolve the flow core, the Matlab algorithm was modified to geometrically construct the boundary layers to a specified size. Figure 4 shows the results of a grid sensitivity where y^+ values were maintained constant at 31.13 for all wall adjacent elements. With the recorded parameters showing very little change with increasing

core flow grid density, Figure 4 demonstrates the dominant influence of the boundary layer in resolving heat transfer problems, especially for slow moving media.

Following the grid sensitivity study, a combined mesh density of 12 elements/cm^2 (or 8.0 and 13.2 for the inner pipe and annulus respectively) was adopted during the optimization study, approximately half the mesh density recorded in [30]. These mesh densities were seen to provide a credible resolution of the core flow within manageable solution times. During the optimization the correct boundary layer thickness was established for each pipe diameter set with y^+ values between 30 and 35.

5. Results

5.1 Coil properties

Before a pipe diameter optimization was undertaken, an investigation into the coil properties; pitch and NABD, was conducted, see Table 3. The non-dimensional torsion constant was calculated following [27]. In Table 3, HEX *a* was the baseline, effective HEX length for HEXs *a* to *d* was constant at 3.3 m. HEX *b* demonstrated that doubling the pitch reduced the pressure drop for a slight increase in heat transfer rate. HEX *c* demonstrated that doubling the NABD, reduced heat transfer and pressure drop. HEX *d* demonstrated that doubling pipe diameter reduced both pressure drop and heat transfer significantly. Compared with HEX *d*, HEX *e* demonstrated a combination of reducing the pitch and increasing NABD can recover the heat transfer rate after increasing pipe diameters whilst maintaining the same pressure drop.

For this application, coil geometry is restrained by unit compactness i.e. small pitch for smallest overall recuperator length and a specified internal void to house the MGT components. By maintaining a constant diameter for the internal void volume and minimal spacing between each pipe turn, both the pitch and NABD are dependant variables on the pipe diameters, specifically the outer pipe diameter which is optimized to provide the required thermal and hydraulic performance. An in-depth investigation to understand the effects of different flow patterns on the relationship between coil geometry and thermal/hydraulic performance is beyond the scope of this work but has been previously well documented [26] [27] [28].

5.2 Coil diameters

As previously mentioned in Section 5.1, the coil void and spacing between each turn were selected as the independent variables to control the recuperator size with different pipe diameters. The coil void diameter was set at 120 mm and the spacing between each pipe turn was maintained at <5 mm.

Figure 5 shows CFD performance data presented as MGT temperature-based effectiveness (Equation 6) and MGT pressure drop ratio (Equation 12) for various coiled pipe-in-pipe heat exchangers based on the combinations shown in Table 1. Temperature-based effectiveness was used for consistency. However, the more accurate energy-based effectiveness was consistently 3-5 percentage points higher, suggesting actual performance would be slightly better than illustrated.

Comprehensive data sets were collected for 1 and 5 coil turns which generated the performance maps shown in Figure 5. To raise effectiveness, an increase in heat exchanger length was required. Based on the linear D'Arcy-Weisbach pressure drop/pipe length theory, the 63.5 mm outer pipe diameter was selected for further investigation at 10 and 20 turns, for that was the smallest pipe diameter which at those lengths, would have a pressure drop within the target limits set for this application; η_{HEX} = 75%, and, P = 90%.

The optimum pipe combination of 63.5 mm and 44.5 mm seen at 1 and 5 coil turns was again confirmed at 10 and 20 turns. At 20 turns the thermo/hydraulic performance has an inflection point of η_{HEX} = 76.0% and P = 90.4%, slightly better than the target values of P = 90% and η_{HEX} = 75%. For the targets set in this application, the performance potential of the coiled pipe in pipe heat exchanger solution is therefore demonstrated as further increase in pipe length will increase pressure drop below the target value. Thus, the theoretical feasibility of a simple low cost coiled pipe in pipe heat exchanger as a MGT recuperator solution has been demonstrated.

6. Discussion

At 20 turns, the heat exchanger pipe length and coil height were 11.53 m and 1.34 m respectively, however a domestic boiler has approximate dimensions 0.4 m $\times$ 0.4m $\times$ 0.74 m. Maintaining the same heat exchanger pipe length, the coil NABD was increased from 0.184 m to 0.337 m and the number of turns reduced from 20 to 11 to

make better use of the boiler space envelope. At these dimensions pressured drop ratio, P, was 91.53% and heat exchanger effectiveness, η_{HEX}, was 75.88% resulting in a MGT system efficiency of 16%, a 1% increase over the performance target.

Figure 5 shows how effectiveness and pressure drop are affected by pipe diameters. Heat exchanger effectiveness increases asymptotically with pipe length and pressure drop increasing linearly. Small hydraulic diameters, be it the annulus or inner pipe, unsurprisingly increase pressure drop. For a given outside pipe diameter, effectiveness increases with a larger inner pipe and smaller annulus. By selecting the optimum pipe diameter ratio for minimum pressure drop, a higher heat exchanger effectiveness is achieved when pressure drop occurs as a result of increased pipe length rather than a sub-optimal pipe diameter combination. Hence, a pipe-in-pipe recuperator will provide good flexibility when sizing for specified hydraulic and thermal performances, but pipe diameter and heat exchange length will ultimately increase when maximum allowable pressure drops are quite small. Hence recuperator size will reduce when MGT pressure ratio, r_c, is increased as the relative pressure drop will be less for a given magnitude of pressure drop. Taking the 63.5 mm, 44.5 mm pipe combination at 10 turns from Figure 5 yields P =93.29% and η_{HEX} =60.71. Plotting this data on Figure 3, shows the same system performance is achieved with half the recuperator size by increasing system pressure ratio, r_c, from 2.15 to 2.5. This suggests that although a lower pressure drop may be beneficial to reduce unit cost, risk and complexity in terms of bearing platform, it ultimately results in a larger unit size.

Reducing heat exchanger pipe length will lower system efficiency, η_s. If a small system efficiency, η_s, penalty could be accepted the disproportionate nature of the asymptotic relationship between effectiveness and pipe length from Figure 6 could be used to significantly reduce unit size. To illustrate, the pressure drop ratio, P, and heat exchanger effectiveness, η_{HEX}, data shown in Figure 5, was used with Equation 13 to generate Figure 7. The delicate thermo/hydraulic impact on system efficiency of each pipe combination is clearly shown. The benefit of improved effectiveness with increased pressure drop from a smaller hydraulic diameter is advantageous over smaller pipe lengths. But when the pressure drops become a greater challenge, larger hydraulic diameters are required to facilitate heat exchanger

effectiveness over the pipe length. At 5 turns the highest system efficiency was 11.3% which resulted from a pipe diameter combination of 63.5 mm and 50.8 mm, or in other words for a 31% reduction in system efficiency a 75% reduction in unit size can be achieved.

6.1 Non dimensional parameter

A non-dimensional parameter describing the fluid stream in a pipe can be established by;

$$\frac{P\rho LD_{hy}}{\dot{m}^2}\left[\frac{kg\cdot m}{s^2}\right]\left[\frac{kg}{m^3}\right]\left[\frac{m}{}\right]\left[\frac{m}{}\right]\left[\frac{s^2}{kg^2}\right]. \quad \textbf{(14)}$$

As the heat exchange system consists of two fluid streams; inner and annulus or subscript *in* and *an*, the following non dimensional relationship can be generated;

$$\left(\frac{P_{in}\rho_{in}L_{in}\dot{m}_{an}^2}{P_{an}\rho_{an}L_{an}\dot{m}_{in}^2}\right)\frac{D_{hy,in}}{D_{hy,an}}=\left(\frac{P_{in}P_{in}R_{an}T_{an}L_{in}\dot{m}_{an}^2}{P_{an}P_{an}R_{in}T_{in}L_{an}\dot{m}_{in}^2}\right)\frac{D_{hy,in}}{D_{hy,an}} \quad \textbf{(15)}$$

For each fluid stream: mass flow, pipe length and gas constants are equal, such that: $\dot{m}_{an}=\dot{m}_{in}$, $L_{an}=L_{in}$, $R_{an}=R_{in}$. The following substitutions are also used to make the system relevant to the MGT analysis;

$$P_{in}=P_{06}+\Delta P_{hg}=P_{01}+\Delta P_{hg}$$

$$P_{an}=P_{02}$$

$$t=\frac{T_{an}}{T_{in}}=\frac{T_{02}}{T_{04}}.$$

Using the substitutions above, Equation 15 can be simplified to the non-dimensional parameter shown in Equation 16 which can be used to describe the hydraulic diameter relationship of a coiled pipe in pipe heat exchanger for use as a recuperator in a MGT application;

$$\Phi=\left(\frac{\left(P_{01}+\Delta P_{hg}\right)^2 t}{P_{02}^2}\right)\frac{D_{hy,in}}{D_{hy,an}} \quad \textbf{(16)}$$

Whilst pitch and NABD have a significant impact on thermal/hydraulic performance as described earlier in Section 5.1, Equation 16 doesn't extend to changes in these

parameters since those terms are not present in the equation. Using additional data sets collected for outer pipe diameters of 88.9 mm and 44.5 mm, Figure 8 plots the pressure drop ratio, P, and heat exchanger effectiveness, η_{HEX}, vs. the non dimensional parameter, Φ, for a single pipe turn. The optimum pipe diameter combination for minimum pressure drop is seen to exist at around, Φ=0.2, whilst maximum heat exchange effectiveness occurs with smaller Φ values and smaller outside pipe diameters as previously suggested.

Considering, the non dimensional parameter, Φ, is a function of the hydraulic diameters, Figure 9 was produced to show the relationship simply between pipe diameters rather than hydraulic diameters for a single pipe turn. Again an optimum pipe diameter combination is seen for inner pipe diameters that are approximately 65% - 75% of the outer pipe diameter.

7. Conclusion

Slow moving media introduced conflicting mesh density requirements on the pipe wall for CFD calculations. A definitive solution was established by modelling separate geometric volumes to accurately resolve the boundary layer by satisfying the y^+ criteria for k-ε semi-empirical near wall treatment. After successfully resolving the boundary layer by satisfying the y^+ criteria, a grid sensitivity study on the core flow showed little change in pressure and temperature between inlet and outlet hence demonstrating that correct modelling of the boundary layer is fundamental to obtaining accurate, grid independent results.

A coiled pipe-in-pipe recuperator solution for a 1 kW MGT DCHP unit was established. The recuperator size was within the acceptable space envelope for a domestic wall-hung boiler but the use of a low MGT pressure ratio, the outcome of using a turbocharger oil cooled journal bearing platform, meant unit size was much bigger than anticipated. Raising MGT pressure ratio from 2.15 to 2.5, would half the heat exchanger volume whilst achieving the same MGT system performance. Alternatively a drop in system efficiency to from 16.3% to 11.3% could facilitate a 75% reduction in unit size.

An optimum pipe diameter combination for minimum pressured drop was consistently observed across different pipe diameters, and coil turns. It was found when translated into a non-dimensional parameter, Φ, based on the ratio of inner and annulus hydraulic diameters, minimum pressure drop occurred at around, Φ = 0.2 for

various pipe diameter combinations. A further relationship was established expressing inner pipe diameter as a percentage of outer pipe diameter. Here an optimum for minimum pressure drop was found when inner pipe diameter was between 65% and 75% of the outer pipe diameter. Heat exchanger effectiveness increased with smaller hydraulic diameters and more specifically smaller annulus cross sectional areas.

When assessing thermal/hydraulic performance, higher heat exchanger effectiveness was achieved when the pressure drop occurred by virtue of pipe length when an optimum or minimum pressure drop pipe diameter combination is used. This is ultimately the most efficient method of achieving increased heat exchanger effectiveness for a pressure drop penalty.

Following the baseline theoretical investigation, experimental work will examine the effect of turbulence promoters to increase effectiveness by better core flow mixing and boundary layer disruption since pipe torsion, which also promotes turbulence, cannot be increased due to confinements of MGT packaging. Increased effectiveness will improve overall system performance and reduce unit size.

ACKNOWLEDGEMENTS

This project is funded by a CASE award with EPRSC and Worcester-Bosch Thermotechnology

APPENDIX A

Notation

C_{pa}	Specific heat capacity of air	[kJ/kg-K]
C_{pg}	Specific heat capacity of exhaust gas	[kJ/kg-K]
D_{hy}	Hydraulic Diameter	[m]
f	Fuel/Air ratio	
$\Delta\mathrm{H}$	Total enthalpy rise across compressor	[kJ/kg]
$\Delta\mathrm{H}_{53}$	Combustion enthalpy of reaction	[kJ/kg]
η_b	Burner efficiency	[%]
η_c	Compressor efficiency, $\frac{(T_{02s}-T_{01})}{(T_{02}-T_{01})}$	[%]

η_{GEN}	DCHP Generator efficiency, $\frac{W_D}{W_{net}}$	[%]
η_{HEX}	Heat exchanger effectiveness, $\frac{(T_{05}-T_{02})}{(T_{04}-T_{02})}$ (MGT)	[%]
	$\frac{Q_D}{Q_{out}}$ (DCHP)	[%]
η_m	Mechanical efficiency, $\frac{W_{in}}{W_{out}}$	[%]
η_s	Gas turbine thermal efficiency, $\frac{\eta_b W_{net}}{Q_{in}}$	[%]
η_t	Turbine efficiency, $\frac{(T_{03}-T_{04})}{(T_{03}-T_{04s})}$	[%]
L_{an}	Effective heat exchange length of annulus	[m]
L_{in}	Effective heat exchange length of inner pipe	[m]
$\dot{m}_{an}$	Mass flow in annulus	[kg/s]
$\dot{m}_{in}$	Mass flow in inner pipe	[kg/s]
$\dot{m}$	Mass flow	[kg/s]
P	Pressure drop ratio, $\frac{\left(1-\frac{\Delta P_{ha}}{P_{02}}-\frac{\Delta P_b}{P_{02}}\right)}{\left(1+\frac{\Delta P_{hg}}{P_{01}}\right)}$	
Φ	Non dimensional pipe-in-pipe parameter	
P_{01}	Compressor inlet total pressure	[bar]
P_{02}	Compressor exit total pressure	[bar]
$\frac{\Delta P_b}{P_{02}}$	Burner pressure drop	[%]
$\frac{\Delta P_{ha}}{P_{02}}$	Heat exchanger air side pressure drop	[%]
$\frac{\Delta P_{hg}}{P_{01}}$	Heat exchanger gas side pressure drop	[%]
Q_{in}	Gas turbine thermal power input	[kW]
Q_{out}	Gas turbine thermal energy output, $Q_{in}-W_{net}$	[kW]

r_c	Pressure ratio, $\frac{P_{O2}}{P_{O1}}$	
Re	Reynolds number, $\mathrm{Re} = \frac{u_{avg} D_{hy}}{\upsilon_{avg}}$	
R_{an}	Gas constant of fluid within annulus	[J/kg-K]
R_{in}	Gas constant of fluid within inner pipe	[J/kg-K]
t	Non dimensional temperature ratio	[K]
T_{O1}	Compressor inlet total temperature	[K]
T_{O2}	Compressor exit total temperature	[K]
T_{O3}	Turbine inlet total temperature (TIT)	[K]
T_{O4}	Turbine exit temperature	[K]
T_{O5}	Recuperator inlet total temperature	[K]
u_{avg}	Average flow velocity	[m/s]
υ_{avg}	kinematic viscosity	[m/s]
W_{in}	Input gas turbine compressor work	[kW]
W_{out}	Output gas turbine turbine work	[kW]
W_{net}	Net electrical power from gas turbine, $W_{out} - W_{in}$	[kW]
y^+	Dimensionless wall distance	

Acronyms

CASE	Collaborative Awards in Science and Engineering
CFD	Computational Fluid Dynamics
DCHP	Domestic Combined Heat and Power
EPRSC	Engineering and Physical Sciences Research Council
MGT	Micro Gas Turbine
NABD	Neutral Axis Bend Diameter
PISO	Pressure-Implicit with Splitting of Operators
SIMPLE	Semi-Implicit Method for Pressure Linked Equations
SWG	Standard Wire Gauge

References

1. CarbonTrust. *Micro CHP Accelerator Interim Report*. The Carbon Trust Publications 2007 [cited 2010 5th March]; Available from: http://www.carbontrust.co.uk/publications/publicationdetail?productid=CTC726
2. Isomura, K., et al., *Experimental verification of the feasibility of a 100 W class micro-scale gas turbine at an impeller diameter of 10 mm.* Journal of Micromechanics and Microengineering, 2006. **16**(9): p. S254 - S261.
3. Peirs, J., et al. *Experimental verification of compressor performance for an ultra-microgasturbine*. in *The 9th International Workshop on Micro and Nanotechnology for Power Generation and Energy Conversion Applications*. 2009. Wachington DC, USA: Imperial College London.
4. Stevens, T. and M. Baelmans, *Optimal pressure drop ratio for micro recuperators in small sized gas turbines.* Applied Thermal Engineering, 2008. **28**(17-18): p. 2353-2359.
5. powerMEMS. *Ultra micro gas turbine*. 2008 [cited 2008 5th August]; Available from: http://www.powermems.be/gasturbine.html.
6. McDonald, C.F., *Low-cost compact primary surface recuperator concept for microturbines.* Applied Thermal Engineering, 2000. **20**(5): p. 471-497.
7. Nagasaki, T., et al. *Conceptual Design of Recuperator for Ultramicro Gas Turbine*. in *Proceedings of the International Gas Turbine Congress*. 2003. Tokyo: International Gas Turbine Conference.
8. Lagerstrom, G. and M. Xie. *High Performance & Cost Effective Recuperator for Micro-Gas Turbines*. in *Proceedings of the ASME Turbo Exposition*. 2002. Amsterdam, The Netherlands: ASME.
9. IR. *Recuperators for Gas Turbine Engines*. Recuperators - Advanced Thermal Technologies 2004 [cited 2010 29th September]; Available from: http://www.ingersollrandproducts.com/energy/_catalogs/Ingersoll_Rand_Recuperator_spec_037LT.pdf.
10. Yungmo, K. and M. Robert, *Annular Recuperator Development and Performance Test for 200kW Microturbine.* ASME Conference Proceedings, 2003. **2003**(3686X): p. 731-734.
11. Shih, H.-Y. and Y.-C. Huang, *Thermal design and model analysis of the Swiss-roll recuperator for an innovative micro gas turbine.* Applied Thermal Engineering, 2009. **29**(8-9): p. 1493-1499.
12. Tsai, B.-J. and Y.L. Wang, *A novel Swiss-Roll recuperator for the microturbine engine.* Applied Thermal Engineering, 2009. **29**(2-3): p. 216-223.
13. Oswald, J.I., D.A. Dawson, and L.A. Clawley. *A new durable gas turbine recuperator*. in *International Gas Turbine Areoengine Congress*. 1999. Indianapolis, USA: ASME paper no. 99-GT-369.
14. Min, J., et al., *High temperature heat exchanger studies for applications to gas turbines.* Heat and Mass Transfer, 2009. **46**(2): p. 175-186.
15. Prieels, L. and H. Antoine. *The ACTE Spiral Recuperator for Gas Turbine Engines*. in *ASME Turbo Expo 2002: Power for Land, Sea, and Air*. 2002. Amsterdam, The Netherlands: ASME paper no. GT2002-30405.
16. Clay, A. and G.D. Tansley. *A Simple, Low Cost, Micro Gas Turbine Recuperator* in *Seventh International Conference on Flow Dynamics*. 2010. Sendai, Japan: Global COE Program and Institute of Fluid Science, Tohoku University.
17. Saravanamutto, H.I.H., G.F.C. Rogers, and H. Cohen, *Gas Turbine Theory*. 5th ed. 2001, Harlow: Pearson Education Limited. 491.

18. Baelmans, M., et al. *Optimal micro channel recuperators for small-sized gas turbines*. in *Second International Conference on Thermal Issues in Emerging Technologies*. 2008: IEEE.
19. Clay, A. and G.D. Tansley, *An Analysis of Micro Gas Turbines for UK Domestic Combined Heat and Power.* The Institution of Diesel and Gas Turbine Engineers, Power Engineer, 2010. **14**(3): p. 18-34.
20. Stevens, T., F. Verplaetsen, and T. Baelmans. *Requirements for recuperators in micro gas turbines*. in *4th International Workshop on Micro and Nano Technology for Power Generation and Energy Conversion Applications location.* 2004. Kyoto, Japan.
21. Clay, A. and G.D. Tansley, *A micro gas turbine for UK domestic combined heat and power.* Journal of Power and Energy - Part A, 2010. **224**(6): p. 839-849.
22. Visser, W.P.J., S.A. Shakariyants, and M. Oostveen. *GT210-22007 Development of a 3kW micro turbine for CHP applications*. in *Proceedings of ASME Turbo Expo 2010: Power for Land, Sea and Air*. 2010. Glasgow, UK: ASME.
23. Monroe, M.A., et al. *GT2005-68715 Component integration and loss sources in 3-5kW gas turbines*. in *ASME Turbo Expo 2005: Power for Land, Sea and Air*. 2005. Reno-Tahoe, Nevada, USA: ASME.
24. Naphon, P. and S. Wongwises, *A review of flow and heat transfer characteristics in curved tubes.* Renewable and Sustainable Energy Reviews, 2006. **10**(5): p. 463-490.
25. Jayakumar, J.S., et al., *Experimental and CFD estimation of heat transfer in helically coiled heat exchangers.* Chemical Engineering Research and Design, 2008. **86**(3): p. 221-232.
26. Hayamizu, Y., et al., *Experimental study of the flow in helical circular pipes: Torsion effect on the flow velocity and turbulence.* Journal of Thermal Science, 2008. **17**(3): p. 193-198.
27. Yamamoto, K., S. Yanase, and R. Jiang, *Stability of the flow in a helical tube.* Fluid Dynamics Research, 1998. **22**(3): p. 153-170.
28. Yamamoto, K., et al., *Visualization of the flow in a helical pipe.* Fluid Dynamics Research, 2002. **30**(4): p. 251-267.
29. Rennie, T.J. and V.G.S. Raghavan, *Numerical studies of a double-pipe helical heat exchanger.* Applied Thermal Engineering, 2006. **26**(11-12): p. 1266-1273.
30. Kumar, V., et al., *Pressure drop and heat transfer study in tube-in-tube helical heat exchanger.* Chemical Engineering Science, 2006. **61**(13): p. 4403-4416.
31. Kumar, V., et al., *Numerical studies of a tube-in-tube helically coiled heat exchanger.* Chemical Engineering and Processing: Process Intensification, 2008. **47**(12): p. 2287-2295.
32. Mandal, M.M. and K.D.P. Nigam, *Experimental Study on Pressure Drop and Heat Transfer of Turbulent Flow in Tube in Tube Helical Heat Exchanger.* Industrial & Engineering Chemistry Research, 2009. **48**(20): p. 9318-9324.
33. Bathie, W., W., *Fundamentals of Gas Turbines*. 2nd ed. 1996, Chichester, UK: John Wiley & Sons, Inc.
34. ANSYS, *Fluent users guide release 12.0, section 26.2.1*. 2009, Canonsburg: ANSYS, Inc.
35. Cengel, Y., *Heat and Mass Transfer: A Practical Approach*. 3rd ed. 2006: McGraw Hill Higher Education.

Figure 1 **Sectioned view of an indicative coiled pipe-in-pipe MGT showing layout and component nomenclature. Outer pipe 1, inner pipe 2, cold end outer pipe extension 3, cold end inner pipe extension 4, hot end outer pipe extension 5, hot end inner pipe extension 6, additional cold end outer pipe extension 7, compressor shroud 8, compressor impeller 9, compressor thrust bearing 10, bearing unit 11, common shaft 12, turbine impeller 13, turbine heat shield 14, turbine shroud 15, combustor 16, generator 17, control unit 18.**

Figure 2 **Sectioned view illustrating the nomenclature for the coiled pipe in pipe heat exchanger.**

Figure 3 **Hydraulic (pressure drop value, P) vs. thermal (heat exchanger effectiveness, η_{HEX}) recuperator performance targets for different pressure ratio to achieve a system efficiency, η_s , of 15% using predefined MGT system parameters.**

Figure 4 **Grid sensitivity study on a single turn of 70 mm pitch, 196.2 mm neutral axis bend diameter, with outer pipe diameter of 63.5 mm and 1.218 mm wall thickness, inner pipe diameter of 50.8 mm and 0.711 mm wall thickness. y^+ values are area-weighted surface integrals. Dean number was 7032 for the inner pipe and 16928 for the annulus. Improved boundary layer modelling was achieved using separate single element thick volumes to satisfy wall y^+ conditions to allow k-ε semi empirical calculations on wall boundary.**

Figure 5 **Hydraulic/thermal CFD performance data for various coiled pipe in pipe heat exchangers using different diameter combinations based on standard stock sizes. Lines connecting equal outside pipe diameters are drawn, refer to Table 1.**

Figure 6 **Heat exchanger effectiveness (dark) and pressure drop (feint) vs. pipe length for 63.5 mm outer tube diameter with 50.8 mm (circle), 44.5 mm (square) and 38.1mm (triangle) inner tube diameters.**

Figure 7 **MGT system efficiency when considering different heat exchanger sizes. Figure illustrates performance of the coiled pipe in pipe heat exchanger at 1, 5, 10 and 20 turns using a constant outer pipe diameter of 63.5 mm and inner pipe diameters of 50.8, 44.5 and 38.1 mm.**

Figure 8 **Pressure drop ratio, P , (black) and heat exchanger effectiveness, η_{HEX} , (grey) vs. non dimensional parameter, Φ, at 1 turn. Lines connecting equal outside pipe diameter are drawn. Graph shows optimum or minimum pressure drop occurs at approximately Φ = 0.2.**

Figure 9 **Pressure drop ratio, P, (black) and heat exchanger effectiveness, η_{HEX}, (grey) vs. inner/outer pipe diameter ratio at 1 turn to illustrate optimum pipe diameter ratio for minimum pressured drop. Lines connecting equal outside pipe diameter are drawn. Graph shows optimum or minimum pressure drop occurs when inside pipe diameters are between 65% and 75% of outside pipe diameter.**

Case #	Outer Tube	Thickness	Inner Tube	Thickness
	[mm]	[mm]	[mm]	[mm]
1	88.9	1.218	76.2	1.218
2	88.9	1.218	63.5	1.218
3	88.9	1.218	50.8	0.711
4	88.9	1.218	44.5	0.711
5	76.2	1.218	63.5	1.218
6	76.2	1.218	50.8	0.711
7	76.2	1.218	44.5	0.711
8	76.2	1.218	38.1	0.711
9	63.5	1.218	50.8	0.711
10	63.5	1.218	44.5	0.711
11	63.5	1.218	38.1	0.711
12	63.5	1.218	31.8	0.711
13	50.8	0.711	44.5	0.711
14	50.8	0.711	38.1	0.711
15	50.8	0.711	31.8	0.711
16	50.8	0.711	25.2	0.711
17	44.5	0.711	38.1	0.711
18	44.5	0.711	31.8	0.711
19	44.5	0.711	25.2	0.711

Table 1 **Tube diameter combinations investigated by CFD analysis.**

Table 2 **Temperature, pressure and mass flow quantities used for CFD boundary conditions. Target quantities are shown in italics. Viscosity [35] and density, calculated by ideal gas law, were used in subsequent heat exchanger numerical calculations.**

Table 3 **Tabulated results of torsion investigation into pipe diameter, pitch, bend diameter.**

- Description and analytical discussion of a novel coiled pipe-in-pipe micro gas turbine recuperator.
- Presentation of findings relating to the optimal pipe diameters with respect to pressure drop and heat exchange effectiveness.
- Description of an appropriate sized CFD grid for modelling heat transfer using wall functions.

	Tempertaure [K]	Pressure [Pa]	Mass Flow [kg/s]	Density [kg/m^3]	Viscosity [kg/ms]
In small pipe	1062	104339	0.02	0.34	4.24×10^{-5}
Out small pipe	*617*	*101325*	*0.02*	0.57	3.02×10^{-5}
In annulus	384	217795	0.02	1.97	2.18×10^{-5}
Out annulus	*893*	*211621*	*0.02*	0.82	3.85×10^{-5}

HEX		a		b		c		d		e	
Diameter	[mm]	26.7	42.2	26.7	42.2	26.7	42.2	53.3	84.3	53.3	84.3
Pitch	[mm]	50.0	50.0	100.0	100.0	50.0	50.0	100.0	100.0	85.0	85.0
NABD	[mm]	210.0	210.0	210.0	210.0	420.0	420.0	210.0	210.0	252.2	252.2
Turns		5	5	5	5	3	3	5	5	5	5
Effective pipe length	[m]	3.30	3.30	3.30	3.30	3.30	3.30	3.30	3.30	3.96	3.96
Pressure drop	[Pa]	26610	6380	18191	6021	14517	5147	457	238	495	275
Temperature Change	[K]	297.5	-317.8	300.4	-320.7	284.9	-304.8	208.6	-226.8	235.6	-254.9
Torsion number		0.017	0.012	0.035	0.045	0.006	0.008	0.051	0.065	0.033	0.043
Dean number		9381	14816	9381	14816	6633	10477	6633	10477	6053	9561
Heat transfer rate	[W]	6743		6811		6468		4895		5476	
Actual HEX Effectiveness	[%]	52.7		53.2		50.6		39.3		43.8	
Temp HEX Effectiveness	[%]	48.7		49.1		46.7		35.7		39.9	
Pressure drop ratio	[%]	0.66		0.76		0.79		0.95		0.95	
Recuperator length	[m]	0.25		0.50		0.13		0.50		0.43	
Recuperator height	[m]	0.24		0.24		0.45		0.26		0.31	

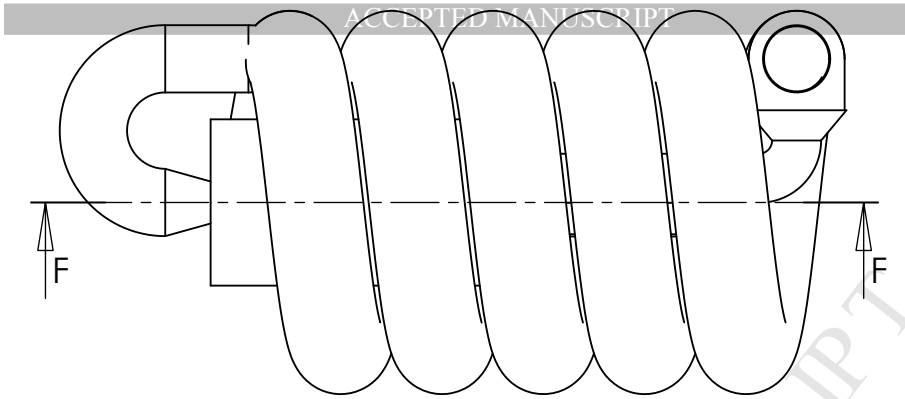

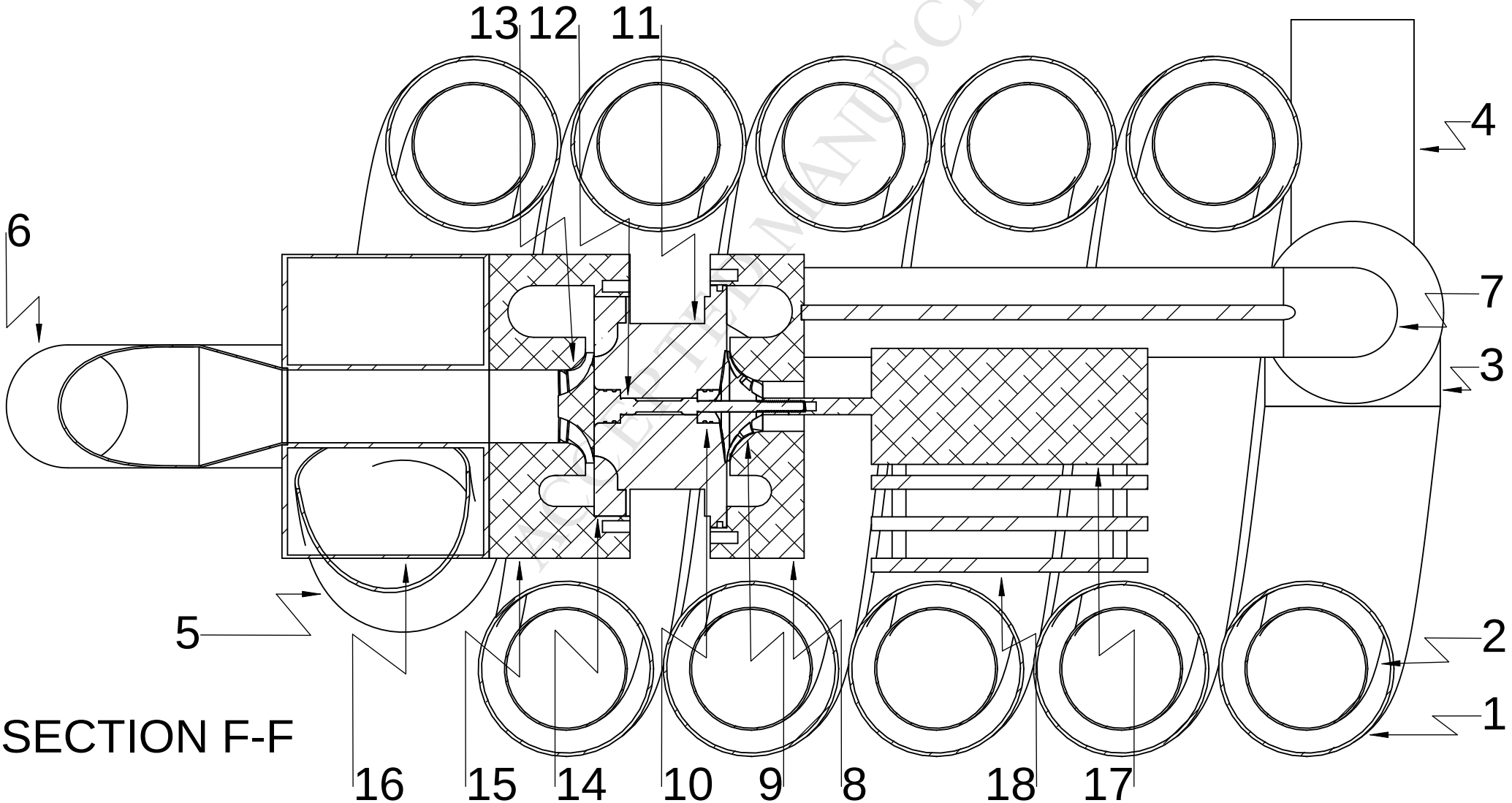

SECTION F-F

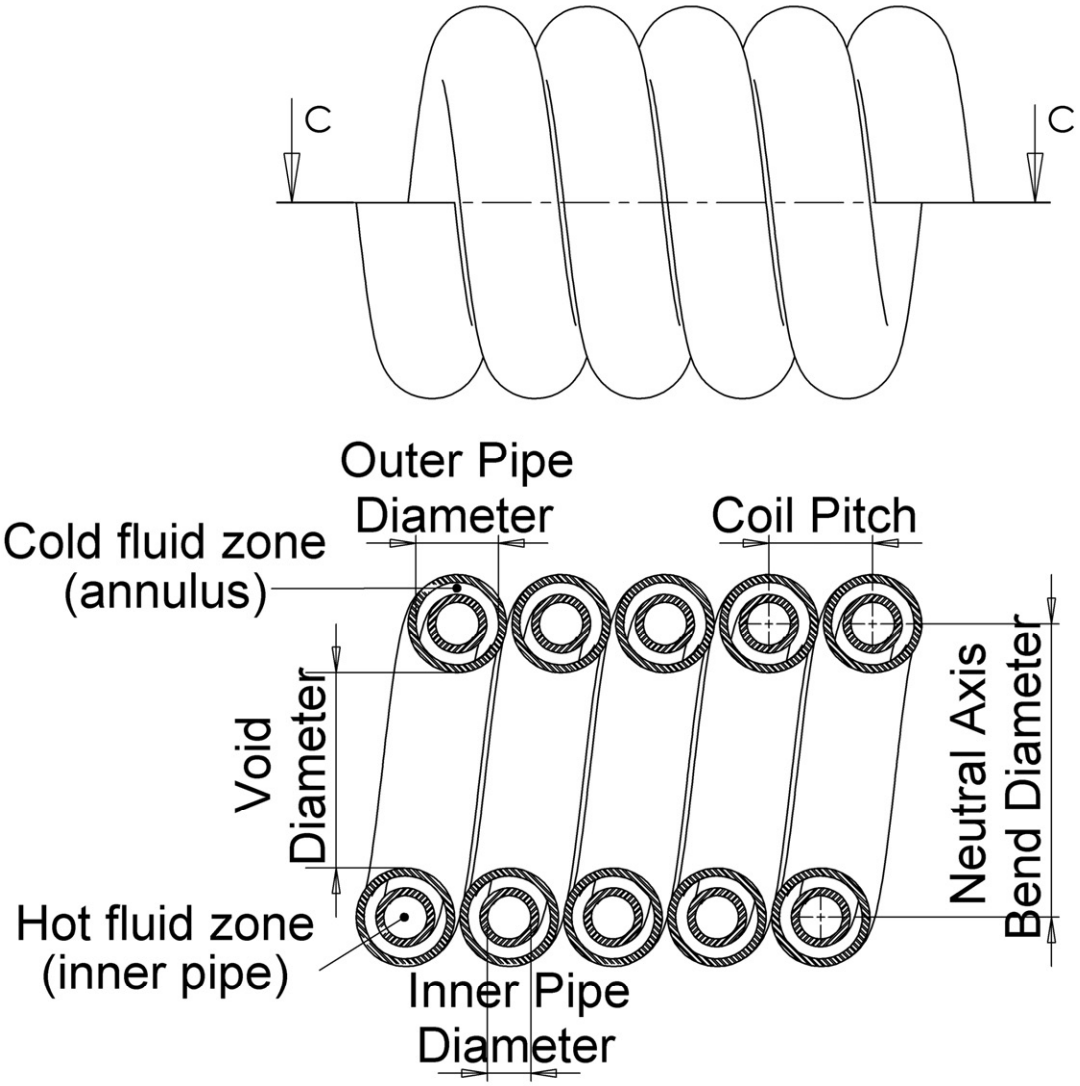
C
C
Outer Pipe Diameter
Coil Pitch
Cold fluid zone (annulus)
Void Diameter
Neutral Axis Bend Diameter
Hot fluid zone (inner pipe)
Inner Pipe Diameter

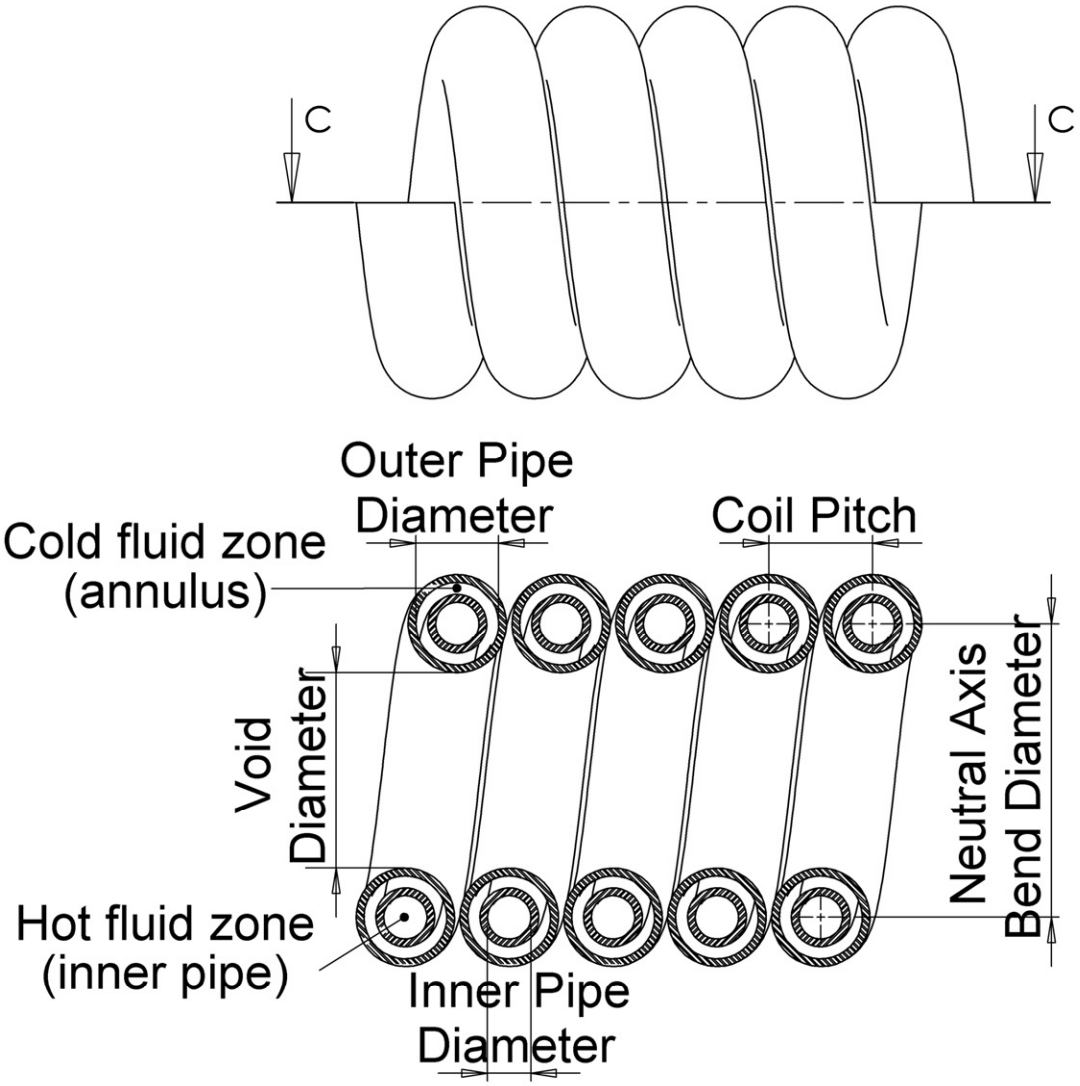
C
C
Outer Pipe Diameter
Coil Pitch
Cold fluid zone (annulus)
Void Diameter
Neutral Axis Bend Diameter
Hot fluid zone (inner pipe)
Inner Pipe Diameter